

# EQCM Studies of Film Growth, Redox Cycling, and Charge Trapping of n-Doped and p-Doped Poly(thiophene)

Ricardo Borjas<sup>†</sup> and Daniel A. Buttry\*

Department of Chemistry, University of Wyoming, Laramie, Wyoming 82071-3838

Received March 19, 1991. Revised Manuscript Received June 17, 1991

The electrochemical quartz crystal microbalance (EQCM) is used to monitor mass changes that accompany the growth, redox cycling, and charge trapping of thin films of poly(thiophene) (PT) at Au electrodes under potentiodynamic conditions. Mechanical conductance spectra of the EQCM/PT composite resonators reveal that the PT films behave as rigid layers, allowing use of the Sauerbrey equation for calculation of quantitative mass changes from the frequency changes recorded with the EQCM. Film growth by oxidation of 2,2'-bithiophene appears to proceed by production of soluble, short-chain oligomers following oxidation, with precipitation as a consequence of both reduction and increasing chain length. Evidence is presented for formation of isolated nuclei during the initial stages of film growth, followed by their coalescence after passage of approximately 0.5–1.5 mC cm<sup>-2</sup> of oxidative charge during electropolymerization. Ellipsometry is used to verify film uniformity across the electrode surface for films with thicknesses between 300 and 1000 Å. Both the n-doping (reductive) and p-doping (oxidative) redox processes are studied in acetonitrile. Relatively stable n-doping is achieved by careful attention to solvent purity. Mass changes during redox cycling indicate that the predominant compositional changes that occur are anion insertion and expulsion during the p-doping process and cation insertion and expulsion during the n-doping process, although small amounts of solvent and/or supporting electrolyte are also transported in both processes. Charge-trapping phenomena are observed for both the n-doping and p-doping processes, with verification of simultaneous counterion trapping provided by the EQCM measurements.

## Introduction

Among their many possible applications, conducting polymers are especially attractive candidates for a variety of battery applications because of both the large amounts of charge they can store and the sometimes high rates at which this charge can be extracted. To achieve high energy and power densities in these applications, the total mass of the cell must be carefully controlled without sacrifice in the rate of charge extraction. This requires a fairly detailed understanding of the transport processes that occur during redox cycling of conducting polymer films, coupled with practical strategies for their manipulation. We have previously described a poly(aniline)/Nafion composite film in which the charge compensating ionic transport during redox cycling was manipulated to achieve faster switching between the insulating and conducting states, a contribution demonstrative of such strategies.<sup>1</sup> Monitoring of the ionic transport processes was accomplished with the electrochemical quartz crystal microbalance (EQCM), and their manipulation was achieved by fabrication of composite film structures.

The EQCM is an ideal tool for the study of compositional changes that occur during redox cycling in thin films of redox or conducting polymers. Several recent, detailed discussions of its use in such applications have appeared.<sup>2,3</sup> It has been successfully applied to studies of the electropolymerization and redox cycling of several conducting polymers including poly(pyrrole),<sup>4</sup> poly(aniline),<sup>5</sup> poly(azulene),<sup>6</sup> poly(3-methylthiophene),<sup>7</sup> and poly(thiophene).<sup>8</sup> It has proven especially useful in the determination of the mechanism and efficiency of film growth for conducting polymers,<sup>4,5</sup> redox polymer films,<sup>9</sup> and other types of deposits,<sup>10</sup> as well as in studies aimed at understanding transport of ions, solvent, and ion pairs or multiplets of supporting electrolyte species within such deposits.<sup>1,3,5,8,11-14</sup> In the present contribution, the EQCM is used to study the growth of films of poly(thiophene) (PT) from bi-

thiophene, the compositional changes that accompany the redox cycling of these films in both the n-doping and p-doping cases, and charge-trapping phenomena and consequent counterion trapping that result from a combination of n- and p-doping closely spaced in time.

## Experimental Section

2,2'-Bithiophene (BTH) was used for the production of the films by electropolymerization. Electropolymerization of thiophene was possible, but the EQCM results for this monomer suggested that dissolution of the underlying electrode material (both Au and Pt were investigated) was occurring at the very positive potentials required for oxidation of this monomer, which prompted the change to BTH. Acetonitrile (ACN, Burdick and Jackson) was used as solvent. The solvent was kept as dry as possible by addition of activated alumina directly into the working electrode compartment of the cell. Tetrabutylammonium and tetramethylammonium hexafluorophosphates (TBAH and TMAH, respectively) were prepared and purified as previously reported,<sup>15</sup> except that all were recrystallized either four or five times. LiClO<sub>4</sub> was carefully ground to a fine powder, spread evenly over a

- (1) Orata, D.; Buttry, D. A. *J. Electroanal. Chem.* **1988**, *257*, 71–82.
- (2) Buttry, D. A. In *Electroanalytical Chemistry. A Series of Advances*; Bard, A. J., Ed.; Marcel Dekker: New York, 1991; Vol. 17, pp 1–85.
- (3) Buttry, D. A. In *In-Situ Studies of Electrochemical Interfaces*; Abruna, H., Ed.; VCH: New York, in press.
- (4) Baker, C. K.; Reynolds, J. R. *J. Electroanal. Chem.* **1988**, *251*, 307–322.
- (5) Orata, D.; Buttry, D. A. *J. Am. Chem. Soc.* **1987**, *109*, 3574–81.
- (6) Borjas, R.; Buttry, D. A., manuscript in preparation.
- (7) Servagent, S.; Vieil, E. *J. Electroanal. Chem.* **1990**, *280*, 227–32.
- (8) Hillman, A. R.; Swann, M. J.; Bruckenstein, S. *J. Electroanal. Chem.* **1990**, *291*, 147–62.
- (9) Hillman, A. R.; Loveday, D. C.; Bruckenstein, S. *Langmuir* **1991**, *7*, 191–94.
- (10) Ostrom, G. S.; Buttry, D. A. *J. Electroanal. Chem.* **1988**, *256*, 411–31.
- (11) Hillman, A. R.; Loveday, D. C.; Bruckenstein, S. *J. Electroanal. Chem.* **1989**, *274*, 157–65.
- (12) Varineau, P. T.; Buttry, D. A. *J. Phys. Chem.* **1987**, *91*, 1292–95.
- (13) Borjas, R.; Buttry, D. A. *J. Electroanal. Chem.* **1990**, *280*, 73–90.
- (14) Lasky, S. J.; Buttry, D. A. *J. Am. Chem. Soc.* **1988**, *110*, 6258–60.
- (15) Fry, A. J.; Britton, W. E. In *Laboratory Techniques in Electroanalytical Chemistry*; Kissinger, P. T., Heineman, W. R., Eds.; Marcel Dekker: New York, 1984; Chapter 13.

<sup>†</sup> Present address: Department of Chemistry, Memphis State University, Memphis, TN 38152.

\* To whom correspondence should be addressed.

Table I. Conductance Data for PT Film during Film Growth<sup>a</sup>

scan	$\Delta f_{\text{fwhh}}$ , Hz	$f_{\text{max}}$ , MHz
0	1180	4.950 609
4	1180	4.950 579
43	1180	4.950 379

<sup>a</sup>0.1 M TBAH + 50 mM BTH in ACN. Scan number 0 corresponds to a conductance spectrum taken prior to film growth. The working electrode was at an applied potential of 0.0 V for these measurements.

watchglass, and dried at 100 °C under vacuum for 72 h, then cooled under vacuum, and transferred directly to the electrochemical cell. The cell was of conventional design (H-cell), except that a glass no. 9 vacuum O-ring joint was blown onto its side to allow for the EQCM crystal to be sandwiched between two O-rings in such a way that only one side was exposed to the solution. Also, the cell contained a Luggin capillary to reduce the uncompensated resistance between the working and reference electrodes. The reference electrode was a Ag wire immersed in a solution of the supporting electrolyte containing 0.04 M AgClO<sub>4</sub>, separated from the working compartment by a porous glass plug. Ferrocene appears at +0.08 ± 0.01 V versus this reference. All potentials are reported versus this Ag/Ag<sup>+</sup> reference. Supporting electrolyte was 0.1 M unless otherwise stated, and monomer solutions were 0.05 M.

Films were prepared under potentiodynamic (i.e., cyclic voltammetric) conditions, with potential limits of 0.0 and 0.8 V. The solution was typically agitated between scans by action of the purging gas (Ar). Film thickness and uniformity were determined by ellipsometry (Rudolf Research, Auto El). The lateral resolution of these measurements was ca. 1 mm. In the dry state, film thicknesses were typically between 300 and 1000 Å, with the uniformity always better than ±15 and ±50 Å, respectively. Good uniformity is important in EQCM studies because the mass sensitivity across the face of the EQCM crystal electrode has a rather strong dependence on the radial distance from the center of the EQCM electrode.<sup>2</sup>

The EQCM apparatus has been described.<sup>2</sup> It allows measurement of mass changes at the electrode surface by virtue of linearly proportional changes in the resonant frequency of the composite resonator comprised of the EQCM crystal and the polymer film deposited onto it. The sensitivity is more than adequate for monitoring compositional changes in the multilayer films investigated here. For this measurement, frequency decreases correspond to mass gain, and vice versa, with the proportionality constant,  $C_f$ , for our instrument being 56.6 Hz cm<sup>2</sup> μg<sup>-1</sup>. The instrumentation for the mechanical impedance measurements has also been previously described.<sup>2,13</sup> Briefly, the impedance measurement consists of the application of an alternating voltage of precisely defined frequency and measurement of the phase and amplitude of the alternating current that flows through the crystal as a consequence of the applied voltage. The resolution for these measurements was typically 20 Hz. These measurements are used to compute various quantities of interest, including the conductance,  $G$  (in Ω<sup>-1</sup> cm<sup>-1</sup>), and the frequency of maximum conductance,  $f_{\text{max}}$  (in hertz), which provides a measure of the total mass deposited during electropolymerization of a given film.<sup>2</sup> To apply the Sauerbrey equation to these films for quantitative calculation of mass changes from frequency changes, it must first be demonstrated that the film behaves rigidly. This is best done by demonstrating that the width of the peak in the conductance spectrum does not change when the film is deposited.<sup>2,13</sup> Below are reported  $\Delta f_{\text{fwhh}}$  (i.e., full width at half-height of the conductance peak in hertz) values that verify that PT behaves rigidly under the experimental conditions used here.

## Results and Discussion

**Film Growth and Rigidity.** Table I shows how the values of  $\Delta f_{\text{fwhh}}$  and  $f_{\text{max}}$  vary with the number of scans into the potential region in which electropolymerization occurs for a PT film that was electropolymerized in 0.1 M TBAH in ACN with 0.05 M BTH at a scan rate of 50 mV s<sup>-1</sup>. These values were measured at an applied potential of 0.0

Table II. Potential-Dependent Conductance Data for PT Film during Growth<sup>a</sup>

scan	$\Delta f_{\text{fwhh}}$ , Hz	scan	$\Delta f_{\text{fwhh}}$ , Hz
0	1080	10	1080
1	1080	10A	1080
3	1080	10B	1220

<sup>a</sup>0.1 M TBAH + 50 mM BTH in ACN. Scan number 0 corresponds to a conductance spectrum taken prior to film growth. All conductance spectra were taken under potential control at 0.0 V, except 10A and 10B, which were taken at +0.85 and -2.33 V, respectively.

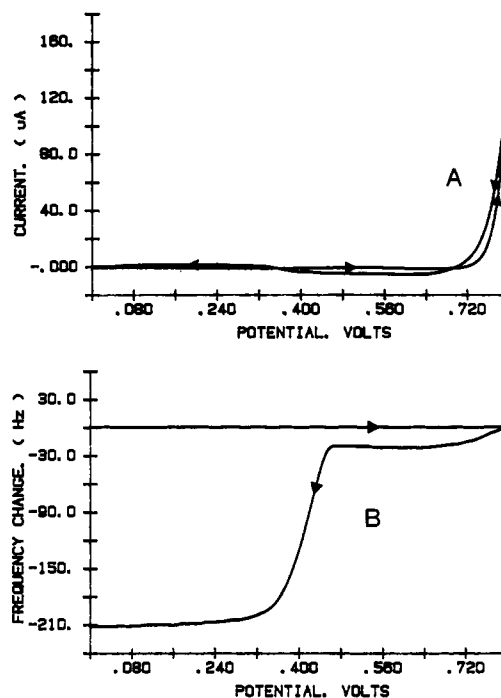
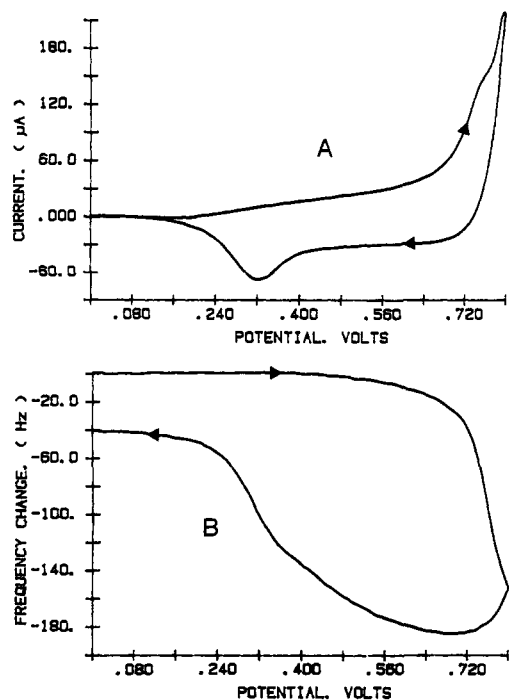


Figure 1. EQCM data for first scan of electropolymerization of BTH: 0.1 M TBAH + 50 mM BTH in ACN; scan rate = 50 mV/s; CV, curve A; QCM, curve B.

V, where the film is in its insulating, undoped state. The constancy of  $\Delta f_{\text{fwhh}}$  with increased film thickness (i.e., the more scans, the thicker the film) shows that the film behaves rigidly under these conditions. Thus, the decrease in  $f_{\text{max}}$  (for a total frequency decrease of 230 Hz) measures the total accumulation of mass at the surface caused by electropolymerization, which was  $4.1 \times 10^{-6}$  g cm<sup>-2</sup>. Note that this mass change was measured after poisoning the electrode potential back to a value at which the polymer was undoped (i.e., neutral), so it represents only the mass of deposited PT plus any supporting electrolyte that might be incorporated into the neutral form of the film.

Table II shows similar data for another film. In this case, the  $\Delta f_{\text{fwhh}}$  values were also determined under potential control at +0.85 V (i.e., in the conducting, oxidized, or *p*-doped state) and a -2.33 V (i.e., in the conducting, reduced, or *n*-doped state). The data reveal that the film is also rigid in its *p*-doped state but not in its *n*-doped state, although the deviation of the  $\Delta f_{\text{fwhh}}$  value from that for the rigid state is much less than has been observed for other types of films.<sup>13,16</sup> In such a case, quantitative calculations of mass changes from frequency data must be interpreted with some caution. The precise origin of these slight deviations from rigid film behavior in the *n*-doped state is unclear at this time. However, it may be related to the relative chemical instability of the film in its *n*-doped state



**Figure 2.** EQCM data for tenth scan of electropolymerization of BTH: 0.1 M TBAH + 50 mM BTH in ACN; scan rate = 50 mV/s; CV, curve A; QCM, curve B.

(e.g., a significant degree of chain cleavage might be expected to induce nonrigid behavior) and the considerable length of time required for obtaining the conductance spectrum (ca. 5 min).

Figure 1 shows an EQCM scan into the potential region in which electropolymerization occurs for a virgin Au electrode. The CV (curve A) shows classic nucleation loop behavior, as expected on the basis of previous studies of PT electropolymerization that indicated nucleation to be a prominent effect in the growth of these films.<sup>17-19</sup> The EQCM frequency response (curve B) shows that a small mass gain occurs following scan reversal but that the majority of the mass gain from this first electropolymerization scan occurs at potentials near those at which the p-doped material is reduced back to the neutral, insulating state. These effects are relatively independent of scan rate, implying that the delayed drop in frequency is a function of applied potential and not the time delay after the oxidation process. The magnitude of the frequency decrease during the first scan will be discussed below.

Figure 2 shows the tenth scan during the electropolymerization of this film. The redox process for the film formed during the previous nine scans is observed, as is the mass gain (loss) due predominantly to anion insertion (expulsion) during oxidation (reduction). In addition to the features from the previously formed film, the net frequency decrease during the scan reveals that additional film has been deposited. Very similar data have previously been reported for a study of the electropolymerization of poly(aniline).<sup>5</sup>

These observations suggest that the process of PT film growth requires that oligomers of sufficient size must be formed prior to the initiation of deposition and that the solubility of the oligomers is much lower in the neutral

**Table III.** Relation of Charge and Frequency Change for Individual Scans during Electropolymerization<sup>a</sup>

$v$ , mV/s	scan	$Q_{ex}$ , mC/cm <sup>2</sup>	$\Delta f_{ex}$ , Hz	$m_2/m_1$
50	1	0.16	210	26
50	5	0.31	51	3.0
50	10	0.70	40	1.2
25	1	0.60	448	15
25	3	0.80	168	4.3
25	6	2.4	121	1.0

<sup>a</sup> 0.1 M TBAH + 50 mM BTH in ACN.  $v$  is scan rate. Data are for two different films prepared at two different scan rates.

than in the p-doped state. These notions are in accord with previous studies of PT electropolymerization,<sup>17-19</sup> which indicated that film formation occurs by formation of oligomers that deposit when they reach a critical value (3-4 units) and that further growth probably occurs from these nuclei. Christensen et al.<sup>20</sup> used FTIR to study PT deposition and redox cycling and found that the thiophene monomer does not adsorb appreciably at Au, again in support of the need for deposition of oligomers (via insolubility) to form nucleation points for further growth.

Another indication of the formation of nuclei in the early stages of film deposition is given by the data in Table III. These data show the variation of the effective mass of the deposit as a function of the number of scans into the region of electropolymerization. The key quantities to compare are the experimentally measured charge consumed in a given scan,  $Q_{ex}$ , and the net frequency decrease for a given scan,  $\Delta f_{ex}$ . These values are used to calculate two effective masses,  $m_1$  and  $m_2$ , respectively, in the following way:

$$m_1 = Q_{ex} MW_{BT} / nF \quad (1)$$

$$m_2 = \Delta f_{ex} / C_f \quad (2)$$

where  $MW_{BT}$  is the molar mass of bithiophene,  $n$  is the number of electrons required to deposit a BT unit into the polymer, and  $F$  is the Faraday constant. The value of  $n$  contains implicitly both the electropolymerization charge efficiency and the electron stoichiometry for film deposition. A value of 2.0 was assumed for these calculations.

The data in Table III are best represented as the ratio of  $m_2/m_1$ . This ratio provides a measure of the degree to which the deposition process makes efficient use of the electrochemical charge consumed in the oxidation of the BT monomer. Inefficient use of the charge would lead to values of  $m_2/m_1$  less than 1.0. This ratio also provides information about the morphology of the deposit. It has been previously shown that for cases in which the deposit morphology is rough enough to cause trapping of supporting electrolyte within pores or between nuclei of the deposit, the mass changes that are calculated from the observed frequency changes can be much larger than expected.<sup>2,10</sup> In the present case, these phenomena would be manifested by a value for  $m_2/m_1$  which is larger than 1.0. It can be seen that for the first few scans,  $m_2/m_1$  is much larger than 1.0, consistent with the production of isolated nuclei which trap considerable amounts of supporting electrolyte between them. However, as the number of scans increases, this ratio approaches 1.0, indicating that (a) the current efficiency for the electropolymerization process is near 1.0 and (b) the morphology of the deposit is such that there is not significant trapping of supporting electrolyte within the film. This variation of the ratio  $m_2/m_1$  with number of scans is exactly what would be expected for the production of isolated nuclei that merge

(17) Hillman, A. R.; Mallen, E. F. *J. Electroanal. Chem.* 1987, 220, 351-67.

(18) Hamnett, A.; Hillman, A. R. *Ber. Bunsen-Ges. Phys. Chem.* 1987, 91, 329-36.

(19) Lang, P.; Chao, F.; Costa, M.; Lheritier, E.; Garnier, F. *Ber. Bunsen-Ges. Phys. Chem.* 1988, 92, 1528-36.

(20) Christensen, P. A.; Hamnet, A.; Hillman, A. R. *J. Electroanal. Chem.* 1988, 242, 47-62.

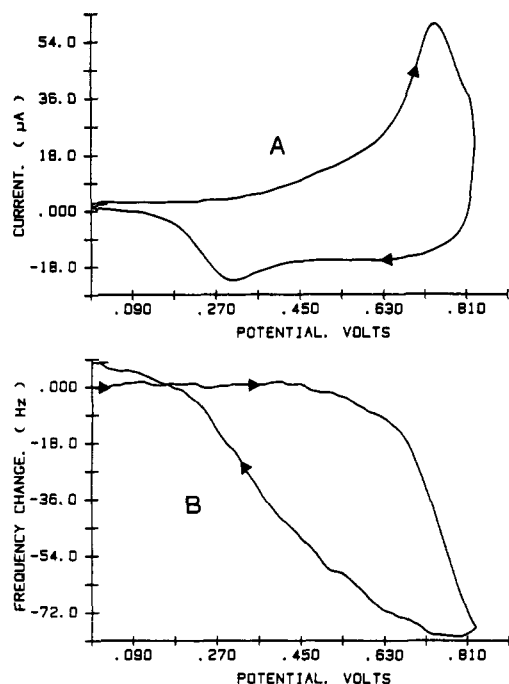


**Figure 3.** EQCM data for thin film of PT in pure 0.1 M TBAH in ACN; scan rate = 50 mV/s; p-doping process; CV, curve A; QCM, curve B.

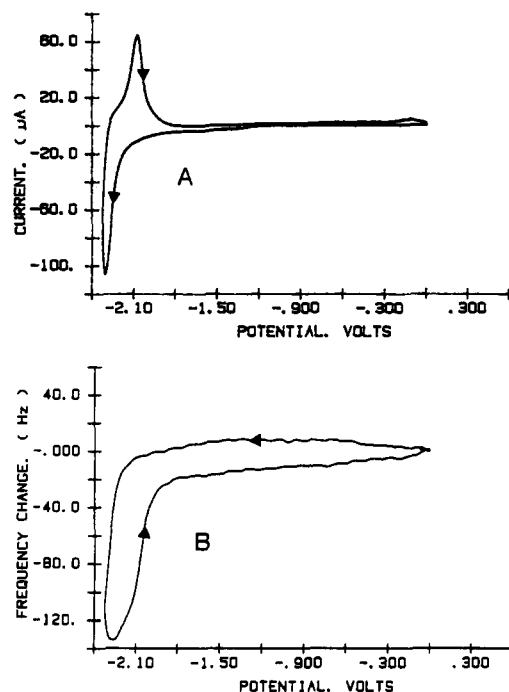


**Figure 4.** EQCM data for thin film of PT in pure 0.1 M TBAH in ACN; scan rate = 50 mV/s; n-doping process; CV, curve A; QCM, curve B.

after further growth and is consistent with the observations reported above and by previous investigators.<sup>17-20</sup>

**Redox Cycling.** Figures 3 and 4 show EQCM scans into the regions for p-doping (oxidation) and n-doping (reduction), respectively, in a solution containing only supporting electrolyte. The observation of stable n-doping has been reported only a few times<sup>21-23</sup> and requires careful

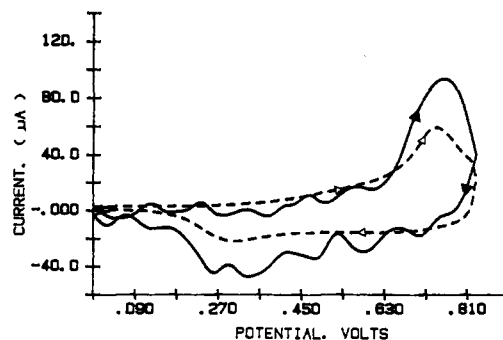


**Figure 5.** EQCM data for thin film of PT in pure 0.1 M TBAH in ACN; scan rate = 50 mV/s; p-doping process. Dashed curve is CV; solid curve is the derivative of the frequency with potential. See text for details.

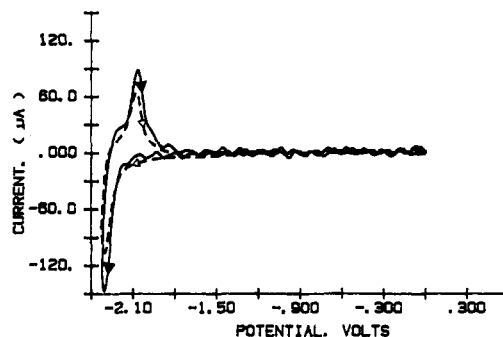


**Figure 6.** EQCM data for thin film of PT in pure 0.1 M TBAH in ACN; scan rate = 50 mV/s; n-doping process. Dashed curve is CV; solid curve is the derivative of the frequency with potential. See text for details.

attention to solvent and supporting electrolyte purity, especially with regard to water content. Also, we note in passing that the presence of even traces of alkali-metal cations in the supporting electrolyte (either intentionally added material or adventitious impurities) causes relatively rapid destruction of the n-doped state. The frequency changes observed during the scans reveal that both doping processes are accompanied by pronounced mass increases and both undoping processes by mass loss. The slight difference between the starting and ending points in Figure 3B is probably from loss of some residual monomer, since this was the first scan after transfer of the film to pure supporting electrolyte.

The hysteresis in the voltammetry is mimicked in the mass changes. Feldberg and co-workers have recently proposed a model for such unusual quasi-reversible (UQR), hysteretic behavior based on phase transformations that accompany the redox process.<sup>24</sup> It seems likely that the insertion of anions during the p-doping and cations during the n-doping processes may be responsible for the phase transformations responsible for this UQR behavior, as pointed out by Feldberg.

Direct comparison of the CV data with the mass data is facilitated by the representation of the mass data in a derivative format.<sup>2,8,10</sup> This method of visualizing the data relies on the direct connection of the removal (insertion) of electrons during the doping process(es) with the insertion of anions (cations) and vice versa during the undoping processes. In this way, subtle differences between the electron and ion-transport processes are more easily seen. Figures 5 and 6 show such plots for the p-doping and n-doping of PT, respectively. The salient feature of the plots is that the mass transported during the redox process

(21) Crooks, R. M.; Chyan, O. M. R.; Wrighton, M. S. *Chem. Mater.* 1989, 1, 2-4.

(22) Mastragostino, M.; Soddu, L. *Electrochim. Acta* 1990, 35, 463-66.

(23) Kaneto, K.; Ura, S.; Yoshino, K.; Inuishi, Y. *Jpn. J. Appl. Phys., Part 2* 1984, 23, 189-91.

(24) Feldberg, S. W.; Rubinstein, I. *J. Electroanal. Chem.* 1988, 240, 1-15.

**Table IV. Charges and Frequency Changes during Redox Cycling for n- and p-Doping**

$\nu$ , mV/s	$\Delta f_n$ , Hz	$Q_n$ , mC/cm <sup>2</sup>	$\Delta f_p$ , Hz	$Q_p$ , mC/cm <sup>2</sup>
25	280	1.95	180	1.44
50	210	1.50	190	1.40
100	175	1.35	180	1.40

is significantly larger than that predicted for simple, unidirectional transport of charge-compensating ions. Hillman et al. have analyzed such behavior in depth for PT films prepared in a slightly different way.<sup>8</sup> In the present case, it suffices to say that this "extra" mass is undoubtedly due to incorporation of small amounts of salt and/or solvent during the doping processes and their expulsion during undoping back to the insulating state.

The mass changes and the charges for cycling several films through their p-doping and n-doping transitions were measured as functions of scan rate. These data are reported in Table IV. From 25 to 100 mV s<sup>-1</sup>, the mass changes and charges were constant for p-doping. On the other hand, both quantities decreased with increasing scan rate for the n-doping process, as shown in the table. The difference in redox cycling transport behavior between the n-doped and p-doped states has been attributed either to differences in counterion diffusion rates for the two processes in PT or to differences in conductivity of the two states.<sup>21</sup> In the present case both TBAH and TMAH gave identical results, indicating that the identity of the cation does not play a major role in determining the transport rates. Thus, we attribute the difference to the much lower conductivity of the n-doped state compared to the p-doped state<sup>21,23</sup> and the consequent decrease in charge propagation rate via electron motion.

**Charge-Trapping Behavior.** Murray and co-workers<sup>25</sup> have studied the charge-trapping effect for bilayers of several different types of polymer systems. The effect is essentially a type of rectification caused by mismatch between the redox potentials of the inner and outer films. In most cases, one of the key criteria for observation of such effects is a redox polymer for the inner film with more than one stable redox couple, so that charging and discharging can occur at separate redox potentials. In cases of this type the phenomenon is conceptually straightforward, and it has been used in a variety of elegant experiments to measure various parameters of interest regarding redox polymer films.<sup>25</sup> However, the phenomenon has also been observed in films that are thought of as uniformly homogeneous, such as poly(3-methylthiophene),<sup>21</sup> and in a benzylviologen film with electrostatically trapped quinones.<sup>26</sup> We have also observed this phenomenon for PT films and discuss the behavior below.

Figure 7 shows a CV of PT in which the negative scan was initiated at 0.0 V, but after first having been scanned into the potential region for p-doping (this initial part of the scan is not shown for clarity). The peak marked A on the CV appears as a prewave on the peak for the n-doping process and corresponds to the release of most of the p-doped charge that had been trapped in the film while in its neutral state. Similarly, the peak marked B appears as a prewave on the peak for the p-doping process. It corresponds to the release of most of the n-doped charge that had been trapped in the film while in its neutral state. These prewaves are not observed unless the film had re-

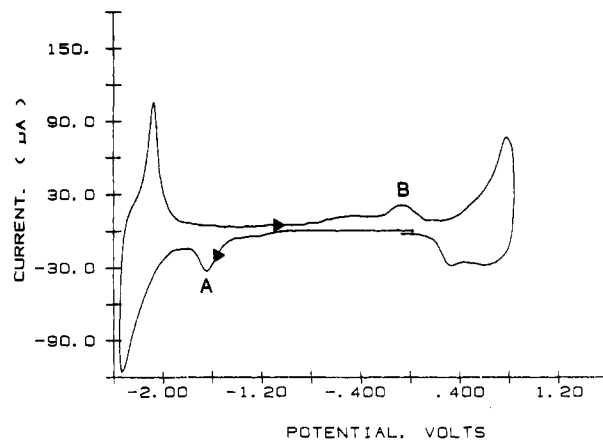


**Figure 7.** CV data showing charge trapping phenomena for PT in pure 0.1 M TMAH in ACN; scan rate = 50 mV/s. Initial potential = 0.0 V; initial scan direction is negative. A scan over the p-doping wave (i.e. up to +0.8 V and back to 0.0 V) occurred just prior to this scan. See text for explanations of peaks A and B.

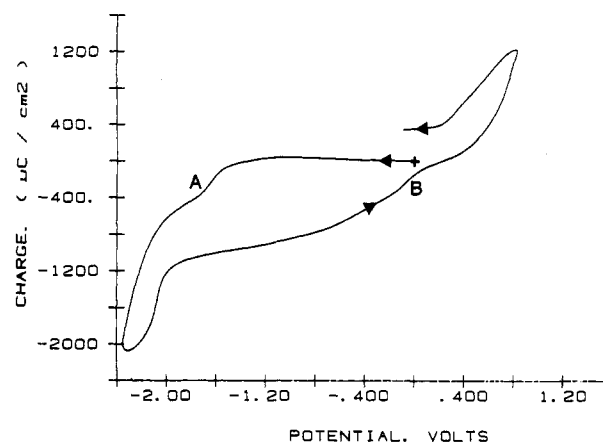


**Figure 8.** Charge versus potential for the scan shown in Figure 7.

cently been scanned to the opposite potential extreme of the scan. The magnitude of the peaks decreases considerably with time, so that they are observed only when the scan to the opposite potential extreme has been fairly recent (e.g., within several minutes).

Figure 8 shows a plot of charge versus potential for the CV in Figure 7; it is simply the integral of that CV. The releases of the trapped charge are marked as A and B, to correspond with the markings in Figure 7. Recall that the scan shown in the figure was run immediately after a prior scan over the anodic, p-doping process. Thus, the starting point in the scan represents a situation in which p-doped charge has already been trapped in the film. If the scan is examined from this starting point, it can be seen that the first cathodic process is release of some of the trapped, p-doped charge, which is labeled in the figure as process A. Measured from the inflection point in the curve, this charge corresponds to about 400  $\mu\text{C cm}^{-2}$ . The next cathodic process is the normal n-doping process, which contributes about 1700  $\mu\text{C cm}^{-2}$  of additional cathodic charge, for a total cathodic charge during the scan of 2100  $\mu\text{C cm}^{-2}$ . The charge immediately recovered after reversal of the scan direction is about 1000  $\mu\text{C cm}^{-2}$ , suggesting trapping of about 700  $\mu\text{C cm}^{-2}$  of n-doped charge in the film. During the positive scan, some of the trapped, n-doped charge is seen to be slowly lost (as shown by the slow increase in charge in the region -1.6 to -0.3 V), but the majority of it is released in the region -0.3 to +0.3 V, coincident with the process labeled B. At this point, there

(25) See, for example: Murray, R. W. In *Electroanalytical Chemistry. A Series of Advances*; Bard, A. J., Ed.; Marcel Dekker: New York, 1984; Vol. 13, pp 191-368.

(26) Hable, C. T.; Crooks, R. M.; Wrighton, M. S. *J. Phys. Chem.* 1989, 93, 1190-92.

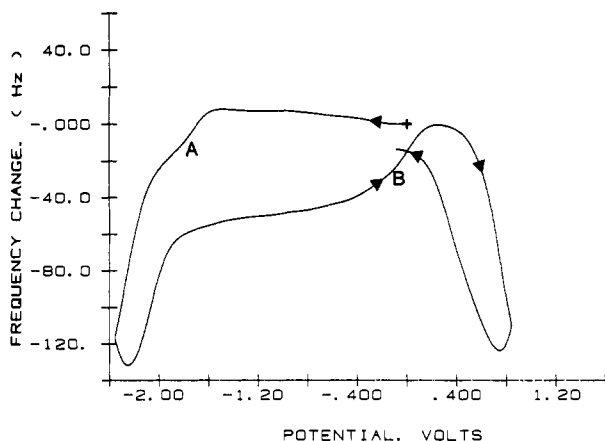


Figure 9. Frequency versus potential for the scan shown in Figure 7.

should be no trapped charge of any kind. Finally, the *p*-doping process occurs, again showing that less charge is recovered during the undoping process than was injected during the doping process.

If charge were completely conserved during the scan (i.e., if all faradaic processes were chemically reversible), then the charge after the B process (during the positive-going, return scan) should be *less than* that at the start of the scan by an amount equal to the trapped, *p*-doped charge. That it is greater than it should be is probably a consequence of some chemical degradation of the film, and consequent loss of mass, during the *n*-doping process. This is perhaps not too surprising due to the known chemical instability of the *n*-doped state.

The amount of charge trapped during *p*-doping and *n*-doping can be obtained from the charges associated with the A and B processes in Figure 8, both of which are near to  $400 \mu\text{C cm}^{-2}$ . If we compare this value with the charges associated with the *p*-doping (ca.  $1200 \mu\text{C cm}^{-2}$ ) and *n*-doping (ca.  $1700 \mu\text{C cm}^{-2}$ ) processes, it becomes clear that the trapped charge represents a significant fraction of the total charge available for the doping processes.

Figure 9 shows the mass changes observed during these charge-trapping events. In the negative scan, there is a slow but significant increase of frequency prior to the prewave. We believe this is caused by the slow release of some of the trapped *p*-doped charge, and a consequent loss of anions. Close inspection of Figure 8 reveals a corresponding slow increase in charge in the same potential region, consistent with this interpretation. An intriguing result is that the frequency change marked A (i.e., from prewave A in Figure 7) corresponds to a mass *gain* rather than a mass loss. This must indicate that the predominant process here is *cation insertion* as opposed to anion expulsion. The detrapping event marked B appears to correspond to a simple release of cations. The frequency attains its original value, indicating that the mass changes that occur during these charge-trapping and -detrapping events are chemically reversible.

An interesting question to address about these data relates to the cause of the cation insertion during the cathodic detrapping event (prewave A). Anion expulsion would seem to be the more preferred process, both because of free volume considerations and because charge compensation in conducting polymers seems to occur by more or less unidirectional transport processes, unless the systems are manipulated to exhibit the opposite behavior. In other words, *p*-doping processes are predominantly accompanied by anion transport and *n*-doping processes are predominantly accompanied by cation transport. How-

ever, there is precedent for effects such as the one observed here.<sup>22,27,28</sup> For example, in the first EQCM study of a conducting polymer, Kaufman and co-workers<sup>27</sup> observed a similar effect during the undoping of poly(pyrrole) in 0.1 M LiClO<sub>4</sub> in tetrahydrofuran solvent. In their case, *p*-doping was accompanied by ClO<sub>4</sub><sup>-</sup> insertion, but undoping was accompanied by Li<sup>+</sup> insertion rather than ClO<sub>4</sub><sup>-</sup> expulsion. This was attributed to strong ion pairing between the cationic sites on the *p*-doped poly(pyrrole) chains and the ClO<sub>4</sub><sup>-</sup> anions, induced by the very low dielectric constant within the film interior. The solvent was implicated in the behavior, because no such effect was observed when ACN was used as solvent. Similar effects have also been recently reported for a different poly(pyrrole) situation.<sup>28</sup> We suspect a similar origin for the effects we have observed for PT films. Thus, strong ion pairing between cationic, *p*-doped sites on the PT chains and their PF<sub>6</sub><sup>-</sup> counterions may cause cation insertion rather than anion expulsion during the detrapping event marked A. However, we have no information regarding whether this event is a kinetic or thermodynamic consequence of such ionic interactions. Scan rate studies would seem to be a relatively simple way to determine this, but the instability of the charge-trapped state of PT precludes such experiments at scan rates low enough to perhaps observe deviations from the behavior observed so far. However, we speculate that the effect is predominantly kinetic, both because of free-volume arguments (i.e., cation insertion requires swelling of the film) and because studies by us and others indicate that, at equilibrium, neutral PT films do not contain much solvent or supporting electrolyte.<sup>8,18-20</sup> Also, whatever the origin of these effects, they must be sensitive to the chemical nature of the anion and cation, because the mass-transport processes that occur during detrapping are not symmetric for the *n*- and *p*-doped states.

## Conclusions

These EQCM studies of film growth, redox cycling, and charge trapping in PT have demonstrated that (1) film growth occurs by nucleation and eventual coalescence of the initially formed nuclei, a process easily observed with the EQCM,<sup>2,10</sup> (2) the mass-transport processes that occur during redox cycling are predominantly, but certainly not exclusively,<sup>8</sup> accompanied by permselective, unidirectional ion transport to achieve charge compensation, and (3) charge-trapping/detrapping events occur for PT films, and the EQCM method provides a rather unique tool with which to study these processes.

The observation of ion transport in unexpected directions during detrapping of *p*-doped charge leads one to conclude that strong ionic interactions prevail inside these low-dielectric-constant media and that these interactions can influence the charge compensation processes that occur for films of conducting polymers and other materials that require ionic charge compensation. Understanding and manipulating these ionic interactions will be important in many applications of these materials because of the known dependence of conductivity on ion pairing (the so-called "charge-pinning" effect).<sup>29</sup>

Another interesting aspect of these data is that the charge trapped during *n*- and *p*-doping is very similar and fairly large with respect to the total doping charge. This large degree of charge trapping may have important practical implications for applications requiring rapid

(27) Kaufman, J. N.; Kanazawa, K. K.; Street, G. B. *Phys. Rev. Lett.* 1984, 53, 2461-64.

(28) Qiu, Y.; Reynolds, J. *Polym. Eng. Sci.* 1991, 31, 417-21.

(29) Frommer, J. E. *J. Macromol. Sci. Chem.* 1987, A24, 449-454.

charge/discharge cycles, but it may also reveal something about the relative homogeneity of these films. For example, the fact that the charge trapped during n- and p-doping is very similar in magnitude may suggest that this charge is trapped in the same region(s) of the film, suggesting the possibility of considerable heterogeneity within the film. Trapping via a homogeneous mechanism (e.g., trapping by isolation from the underlying electrode by the intervening polymer layer, which becomes insulating first during the undoping process<sup>21</sup> seems unlikely in this case, because it should depend on the film conductivities, which are known to be at least 2 orders of magnitude different for the n- and p-doped cases.<sup>21,23</sup> Also, careful ellipsometric studies of the mode of doping for poly(aniline), another (albeit, different) conducting polymer system, indicate uniform doping and undoping.<sup>30</sup> Thus, in the present case, trapping via a mechanism involving film heterogeneity seems more likely. We suggest that there are regions of these films that are in relatively poor physical contact with

the bulk of the film and that the deswelling (caused by ion expulsion) that occurs during the undoping process causes the bulk of the film to draw away from these regions, thus degrading the quality of the electronic contact between them. On doping at the opposite potential extreme, reswelling (due to ionic insertion) occurs, reestablishing the electronic contact needed for efficient release of the trapped charge.

While this suggestion that charge trapping in such materials is caused by film heterogeneity is clearly of a speculative nature, it does suggest that microscopic investigations of such films are in order. Such studies are facilitated by the ability to make various types of spectroscopic measurements with relatively high spatial resolution, such as FTIR, Raman, fluorescence, etc., and may also be possible with very high resolution probes of electronic structure such as STM, at least at the film surface. We hope that this report will prompt such investigations.

**Acknowledgment.** We are grateful to the Office of Naval Research for the full support of this work.

**Registry No.** Bithiophene (homopolymer), 80029-99-8.

(30) Gottesfeld, S.; Redondo, A.; Feldberg, S. *J. Electrochem. Soc.* 1987, 134, 271-72.

## Conjugated Aromatic Poly(azomethines). 1. Characterization of Structure, Electronic Spectra, and Processing of Thin Films from Soluble Complexes

Chen-Jen Yang and Samson A. Jenekhe\*

Center for Photoinduced Charge Transfer and Department of Chemical Engineering,  
University of Rochester, Rochester, New York 14627-0166

Received March 25, 1991. Revised Manuscript Received July 5, 1991

A series of conjugated aromatic poly(azomethines), poly(1,4-phenylenemethylidynenitrilo-1,4-phenylenenitrilomethylidyne) (PPI), poly(2-methyl-1,4-phenylenemethylidynenitrilo-1,4-phenylenenitrilomethylidyne) (PMPI), poly(1,4-phenylenemethylidynenitrilo-2,5-dimethoxy-1,4-phenylenenitrilomethylidyne) (PMOPI), poly(1,4-phenylenemethylidynenitrilo-2,5-dihydroxy-1,4-phenylenenitrilomethylidyne) (PHOPI), and copolymer PPI/PMPI, have been prepared and solubilized in organic solvents by reversible complexation with either gallium chloride or di-*m*-cresyl phosphate (DCP) and characterized. The molecular structure of the aromatic polyazomethines was characterized by <sup>1</sup>H NMR spectra of the polymers in GaCl<sub>3</sub>/deuterated nitromethane. The conjugated aromatic poly(azomethines) were processed into optical-quality thin films from their soluble complexes in organic solvents and characterized. The solid-state electronic absorption spectra showed that the  $\lambda_{\text{max}}$  for  $\pi$ - $\pi^*$  transition varies from 405 nm for PPI to 497 nm for PHOPI. The corresponding solid-state bandgap was in the range 2.07-2.50 eV. The relatively low bandgap of PHOPI (2.07 eV) compared to PMOPI (2.34 eV) and PPI (2.50 eV) is due to its intramolecular hydrogen-bonding-mediated coplanar structure. Intramolecular hydrogen bonding in PHOPI was further evidenced by FTIR spectra and the results of solubility and complexation studies. The solid-state electronic absorption spectra of complexes of these conjugated aromatic poly(azomethines) were found to exhibit greater electronic delocalization and smaller bandgaps (1.85-2.15 eV) than the pure polymers. Origin of this remarkable red shift of electronic spectra was attributed to complexation-induced change in polymer conformation. The preparation of soluble complexes of conjugated aromatic poly(azomethines) and their processing to optical-quality thin films has now opened up investigation of the solid-state properties of this class of liquid-crystalline conjugated polymers and high-temperature fiber-forming materials.

### Introduction

Conjugated aromatic *p*-phenylene ring polymers occupy a central place in current efforts to elucidate the structure-property relationships of electronic, optical, and

nonlinear optical polymers. Among the well-studied *p*-phenylene ring polymers are poly(*p*-phenylene) (PPP),<sup>1,2</sup> poly(*p*-phenylene sulfide) (PPS),<sup>1,2</sup> polyanilines<sup>3-6</sup> such as

\* To whom correspondence should be addressed.

(1) Frommer, J. E.; Chance, R. R. *Encycl. Polym. Sci. Eng.* 1985, 5, 462-507.